SUPPORTING INFORMATION

Selective Binding of Highly Hydrophilic Anions by Incarceration into Rigidified Nanojars: Sulfate vs. Carbonate

Wisam A. Al Isawi,[a]† Austin Z. Salome,[a]† Basil M. Ahmed,[a] Matthias Zeller[b] and Gellert Mezei[a]*

[a] *Department of Chemistry, Western Michigan University, Kalamazoo, Michigan 49008, USA*

[b] *Department of Chemistry, Purdue University, West Lafayette, Indiana 47907, USA*

†These authors contributed equally to this work

*Corresponding author. Email: gellert.mezei@wmich.edu

CONTENTS **PAGE**

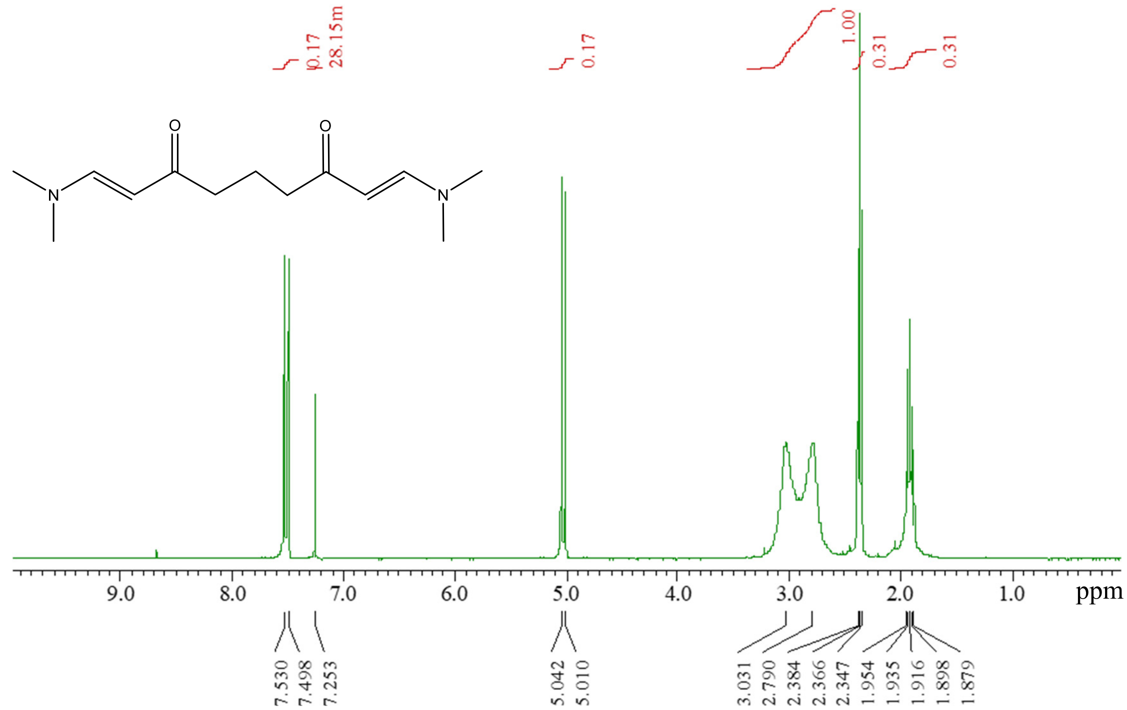

Figure S1. [1]H-NMR spectrum of 1,9-bis(dimethylamino)nona-1,8-diene-3,7-dione in $CDCl_3$.

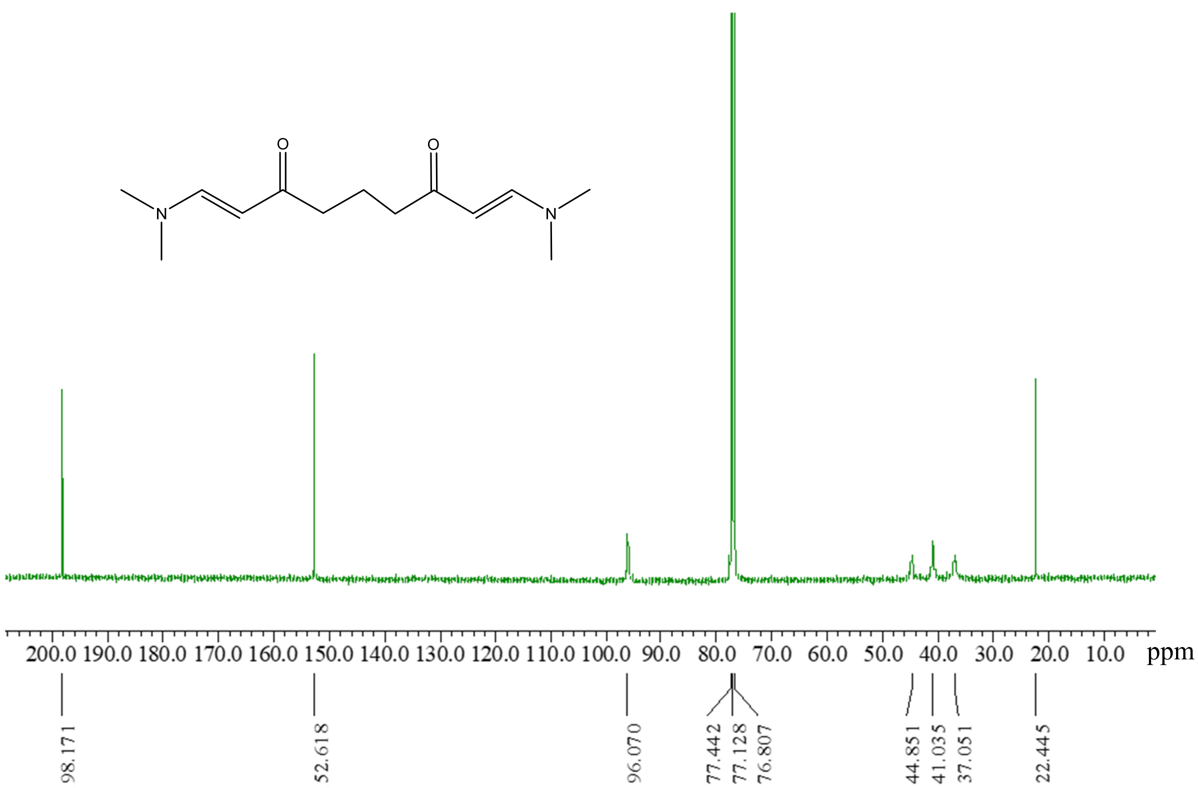

Figure S2. [13]C-NMR spectrum of 1,9-bis(dimethylamino)nona-1,8-diene-3,7-dione in $CDCl_3$.

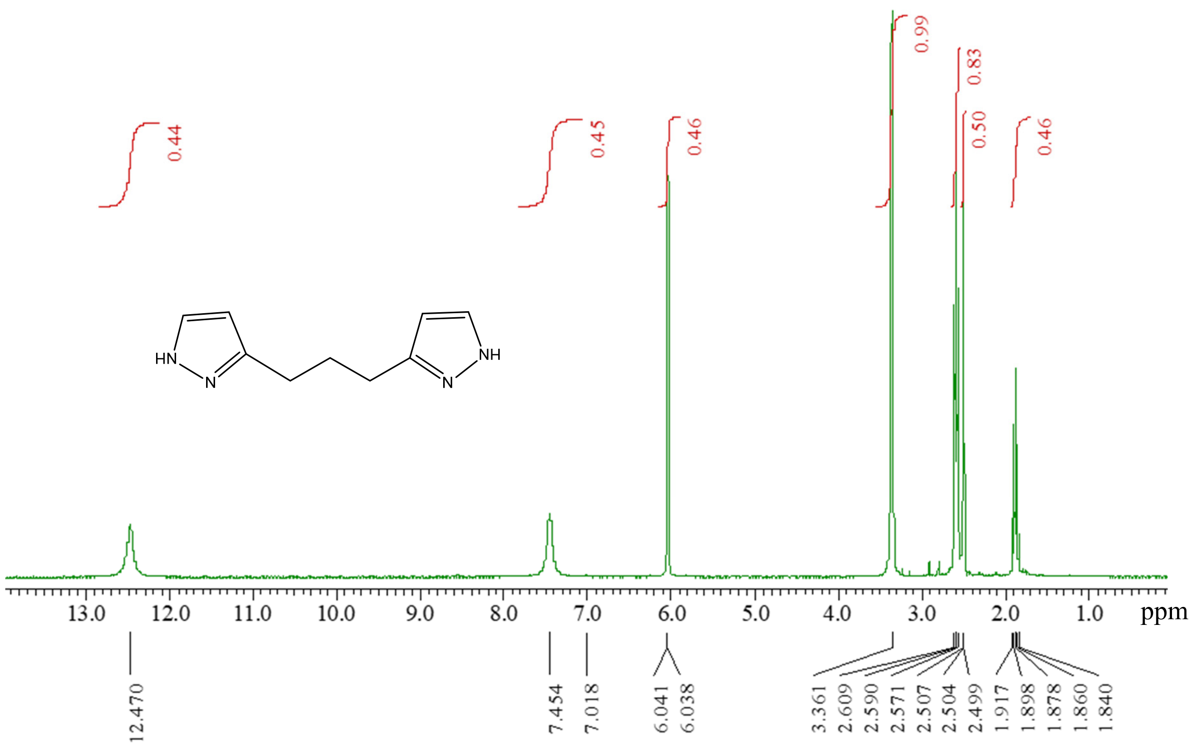

Figure S3. ^{1}H-NMR spectrum of 1,3-di(pyrazol-3(5)-yl)propane in DMSO-d_6.

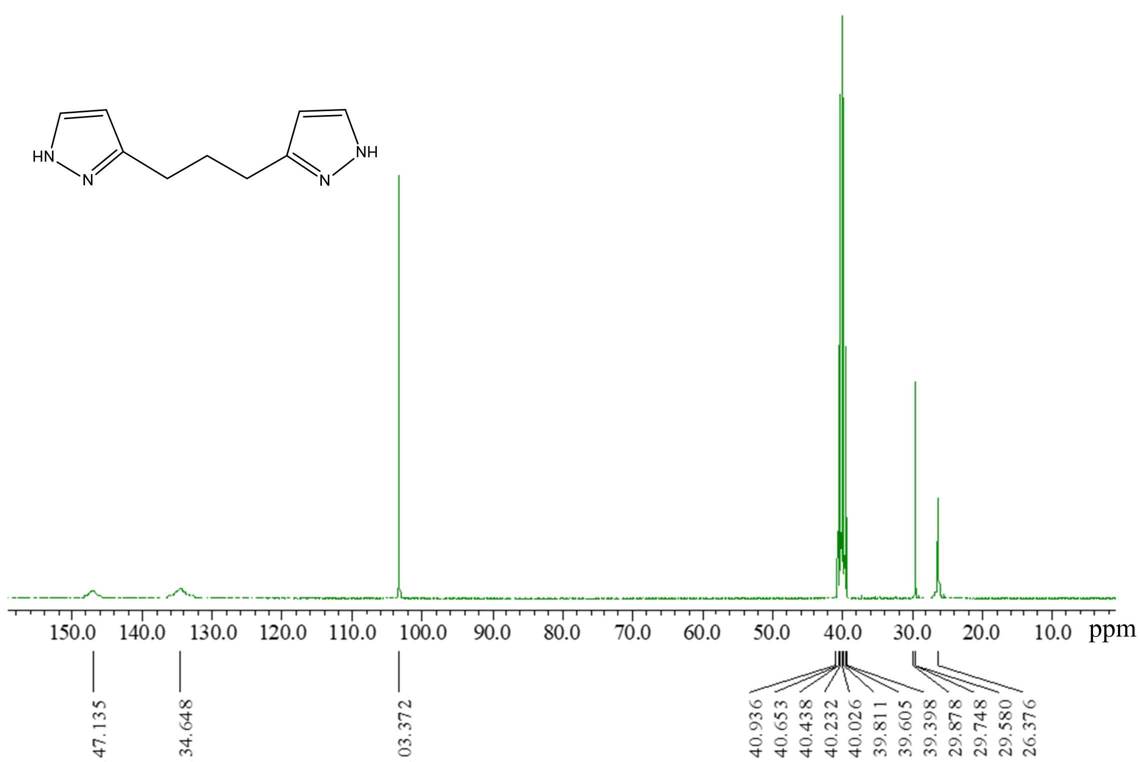

Figure S4. ^{13}C-NMR spectrum of 1,3-di(pyrazol-3(5)-yl)propane in DMSO-d_6.

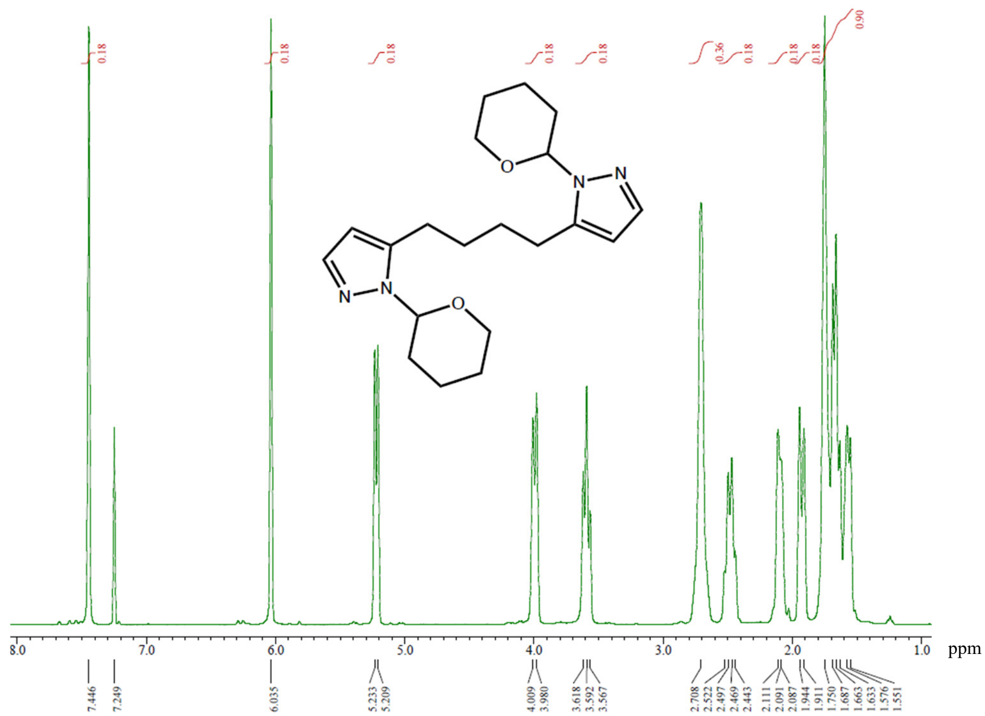

Figure S5. ^{1}H-NMR spectrum of 1,4-bis(1-(tetrahydropyran-2-yl)pyrazol-5-yl)butane in $CDCl_3$.

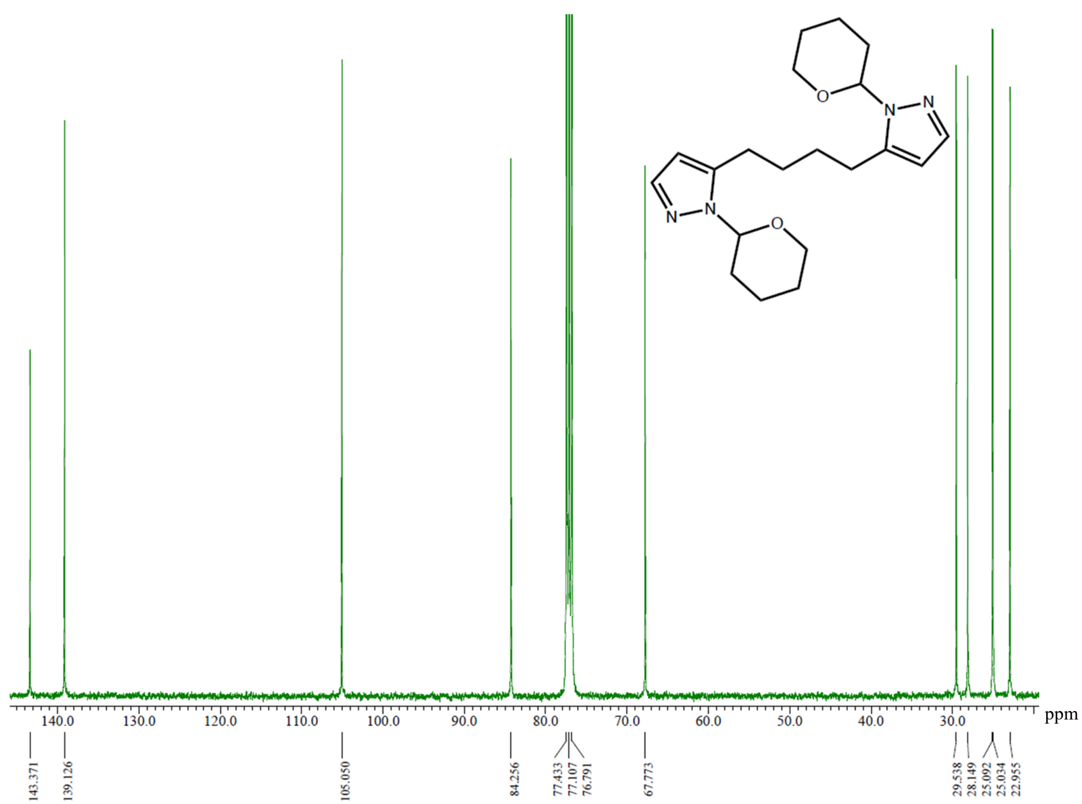

Figure S6. ^{13}C-NMR spectrum of 1,4-bis(1-(tetrahydropyran-2-yl)pyrazol-5-yl)butane in $CDCl_3$.

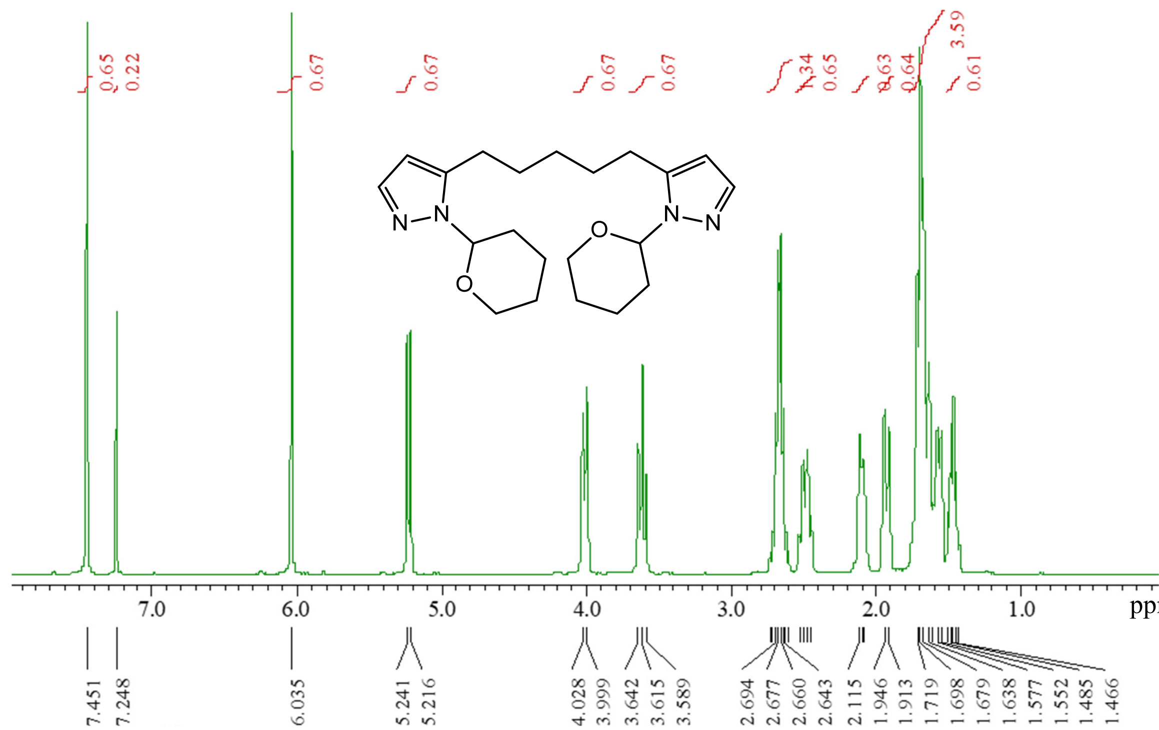

Figure S7. ^{1}H-NMR spectrum of 1,5-bis(1-(tetrahydropyran-2-yl)pyrazol-5-yl)pentane in $CDCl_3$.

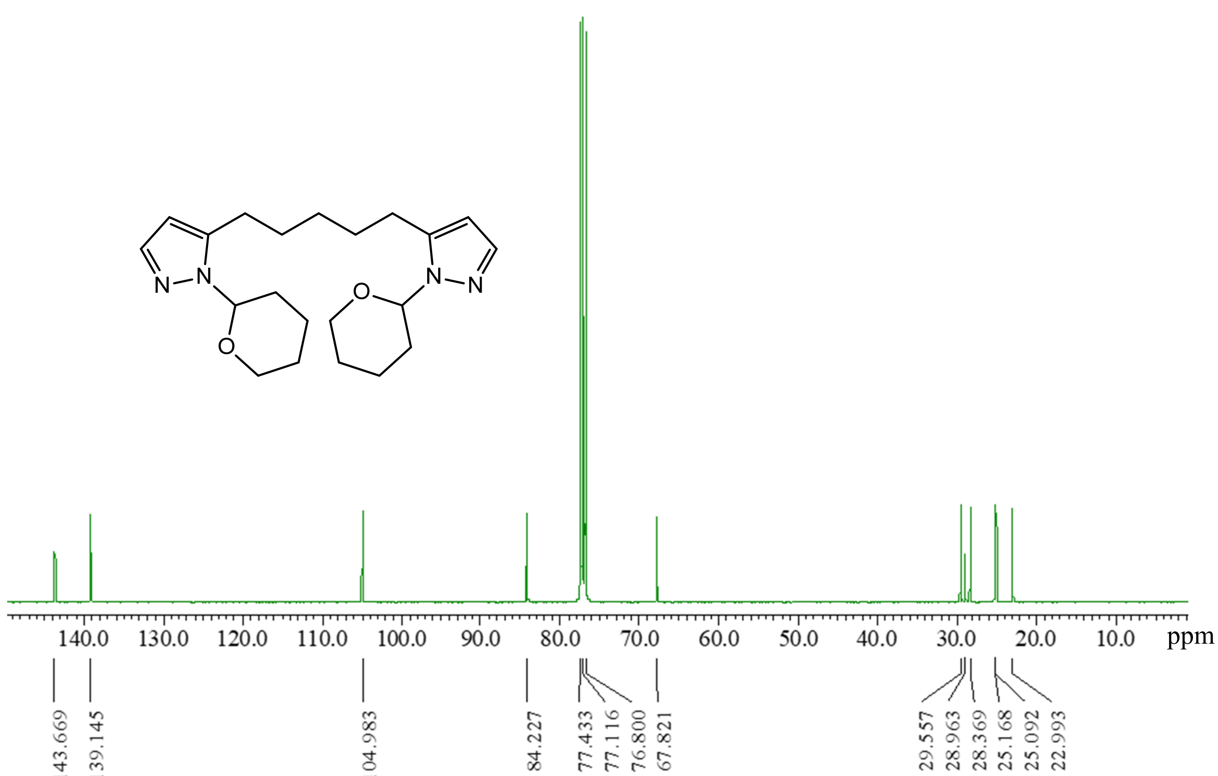

Figure S8. ^{13}C-NMR spectrum of 1,5-bis(1-(tetrahydropyran-2-yl)pyrazol-5-yl)pentane in $CDCl_3$.

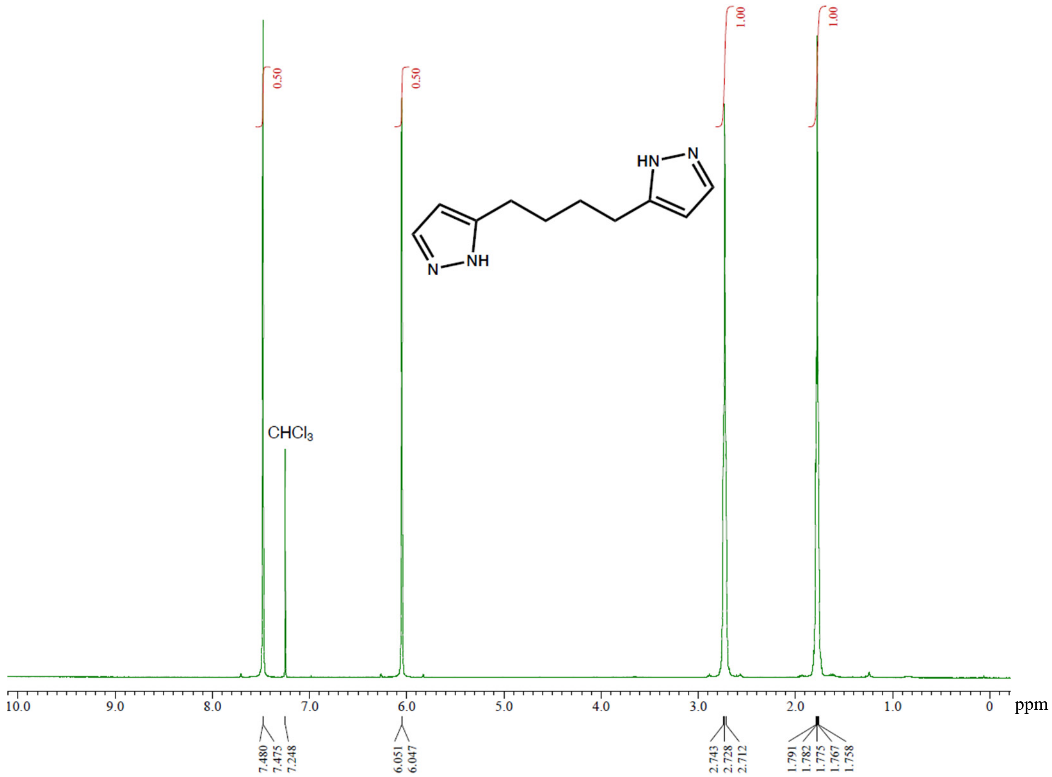

Figure S9. ^{1}H-NMR spectrum of 1,4-di(pyrazol-3(5)-yl)butane in $CDCl_3$.

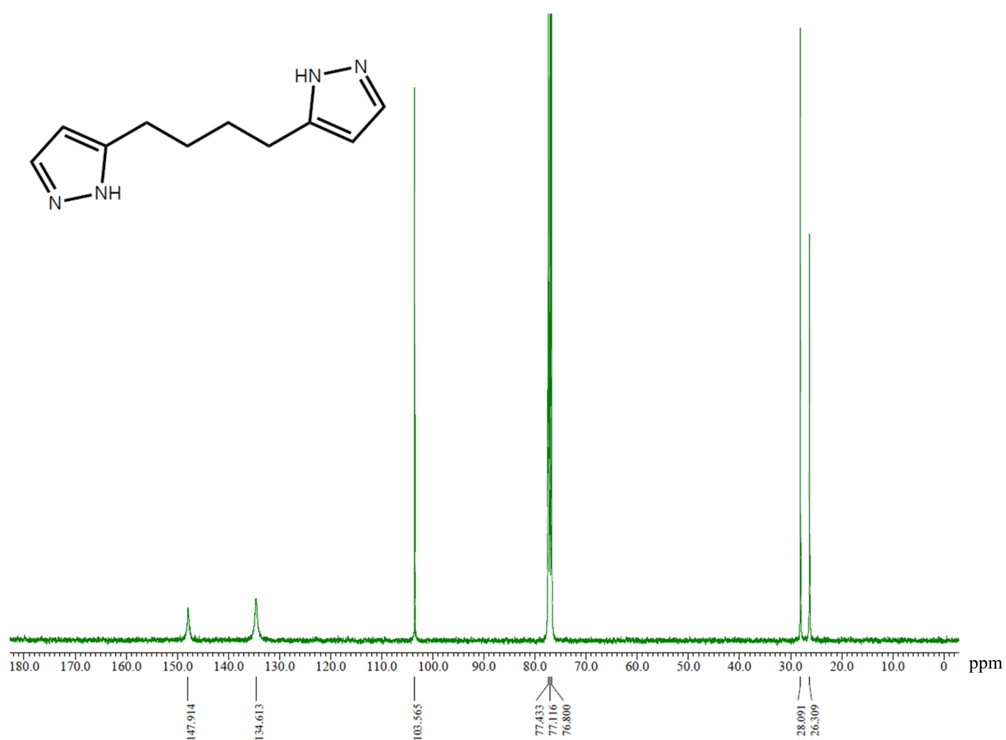

Figure S10. ^{13}C-NMR spectrum of 1,4-di(pyrazol-3(5)-yl)butane in $CDCl_3$.

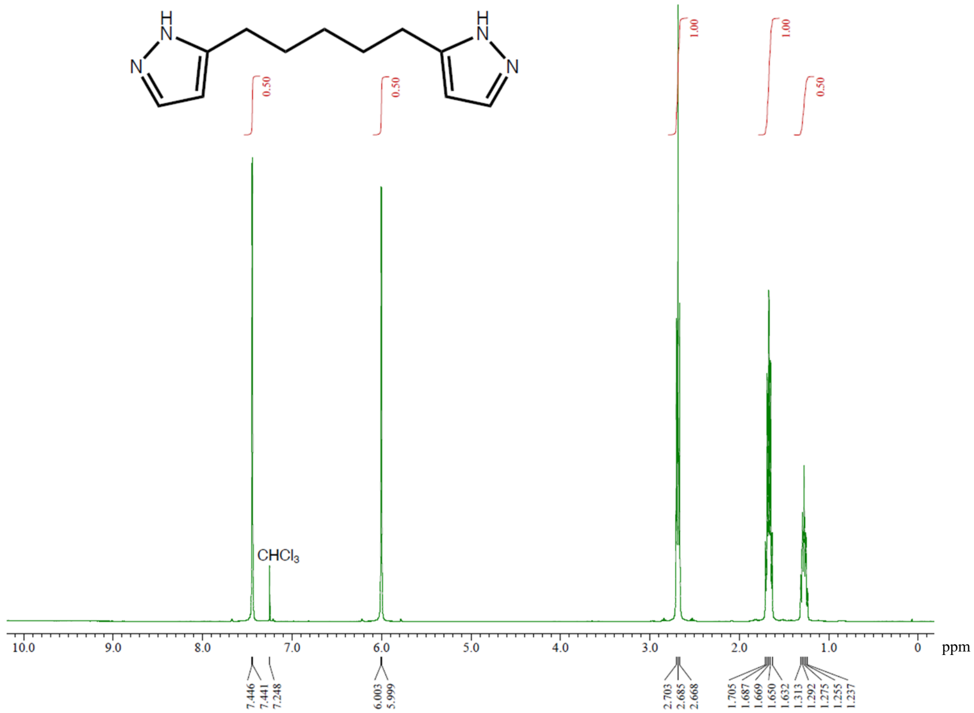

Figure S11. ^{1}H-NMR spectrum of 1,5-di(pyrazol-3(5)-yl)pentane in $CDCl_3$.

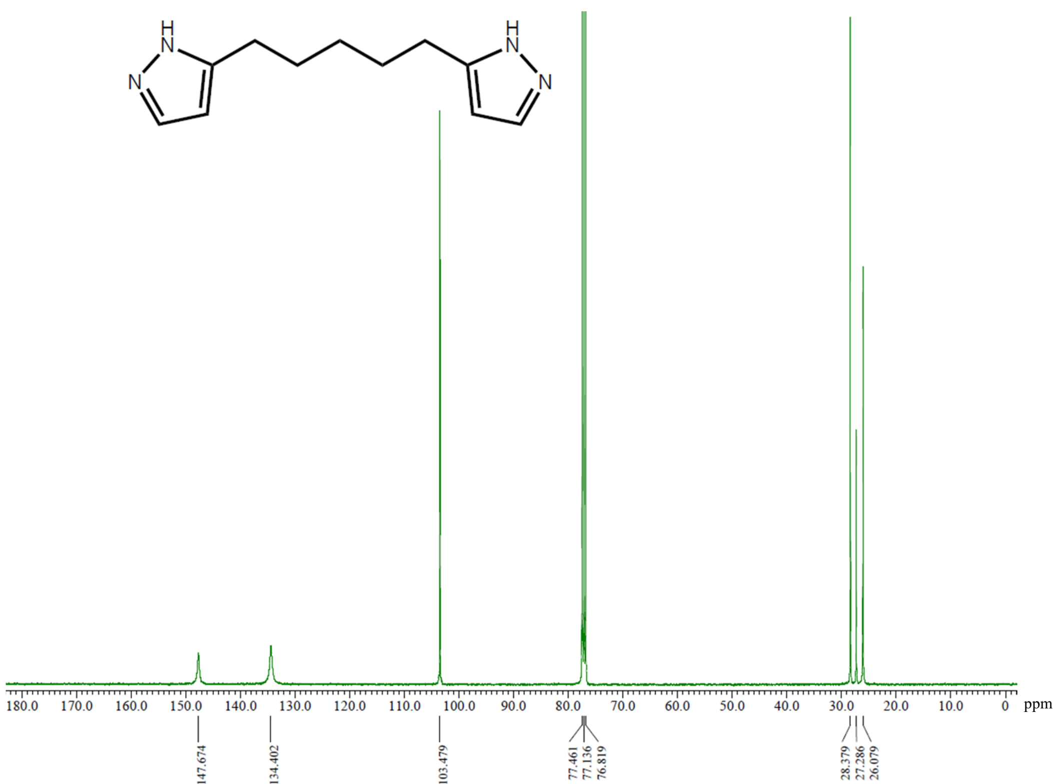

Figure S12. ^{13}C-NMR spectrum of 1,5-di(pyrazol-3(5)-yl)pentane in $CDCl_3$.

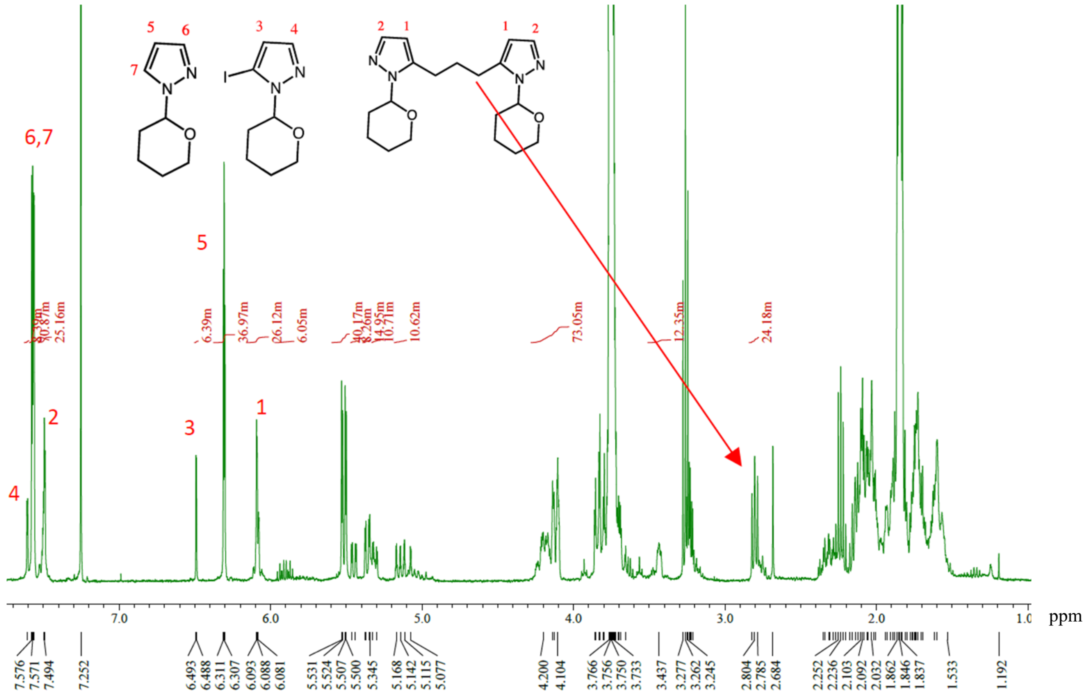

Figure S13. ^{1}H-NMR spectrum of the product obtained from the reaction of (1-(tetrahydropyran-2-yl)pyrazol-5-yl)lithium with 1,3-diiodopropane (2:1 molar ratio) containing ~37% H_2**L3**, ~10% 5-iodo-1-(tetrahydropyran-2-yl)pyrazole and ~53% unreacted 1-(tetrahydropyran-2-yl)pyrazole.

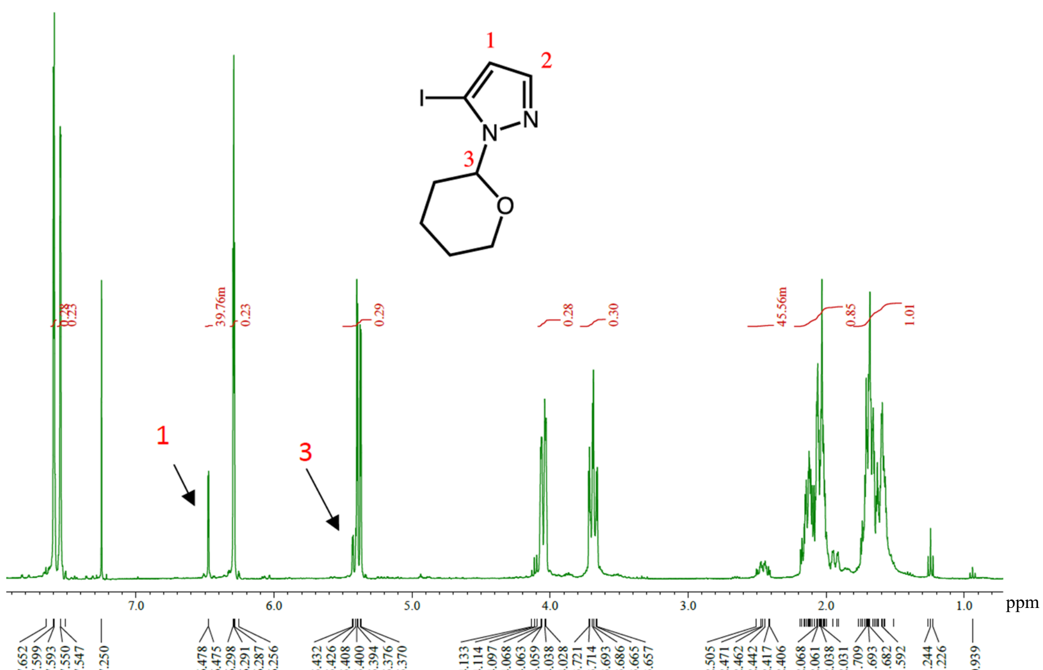

Figure S14. ^{1}H-NMR spectrum of the product obtained from the reaction of (1-(tetrahydropyran-2-yl)pyrazol-5-yl)lithium with 1,2-diiodoethane (4:1 molar ratio) containing ~14% 5-iodo-1-(tetrahydropyran-2-yl)pyrazole and ~86% unreacted 1-(tetrahydropyran-2-yl)pyrazole.

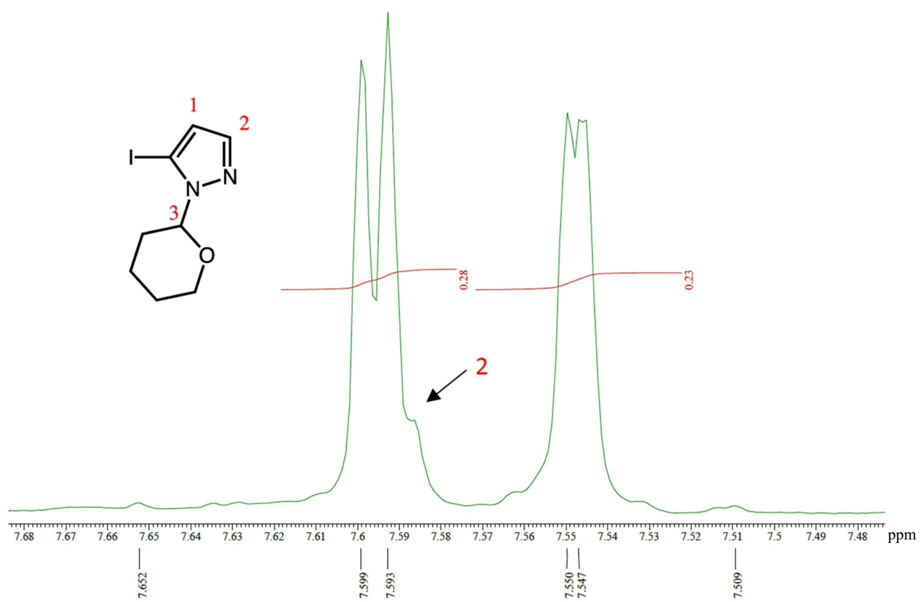

Figure S15. Zoomed-in region of the ^{1}H-NMR spectrum of the product obtained from the reaction of (1-(tetrahydropyran-2-yl)pyrazol-5-yl)lithium with 1,2-diiodoethane (4:1 molar ratio) showing the signal of the proton from the 3-position of 5-iodo-1-(tetrahydropyran-2-yl)pyrazole.

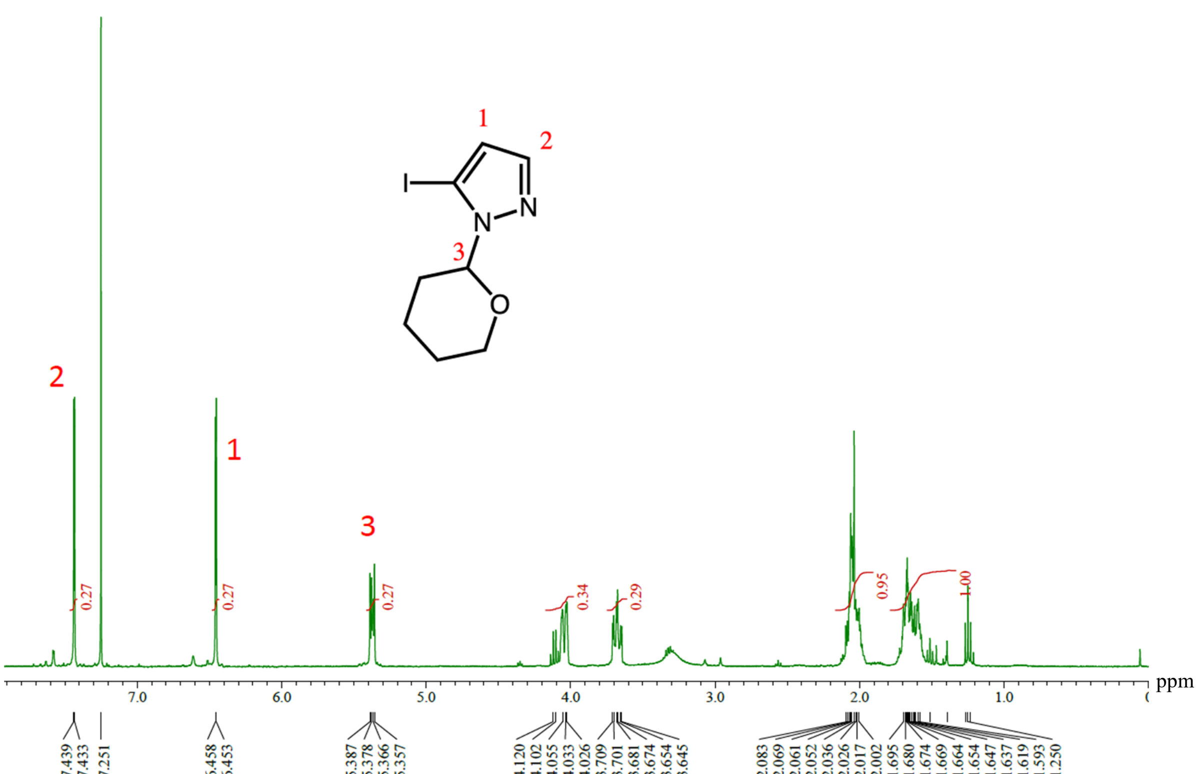

Figure S16. ^{1}H-NMR spectrum of the product obtained from the reaction of (1-(tetrahydropyran-2-yl)pyrazol-5-yl)lithium with 1,2-diiodoethane (1:2 molar ratio) showing almost pure 5-iodo-1-(tetrahydropyran-2-yl)pyrazole.

Table S1. Hydrogen bonding data for H_2**L4**.

D–H···A	D–H/(Å)	H···A/(Å)	D···A/(Å)	D–H···A/°	Symmetry operator for A
N1—H1N···N2	0.91(2)	2.24(2)	2.986(2)	138(2)	−x+1, −y+2, −z+2
N1—H1N···N3	0.91(2)	2.39(2)	3.036(2)	127(2)	x+1, y, z+1
N4—H4N···N2	0.89(2)	2.29(2)	3.127(2)	158(2)	x, y, z−1

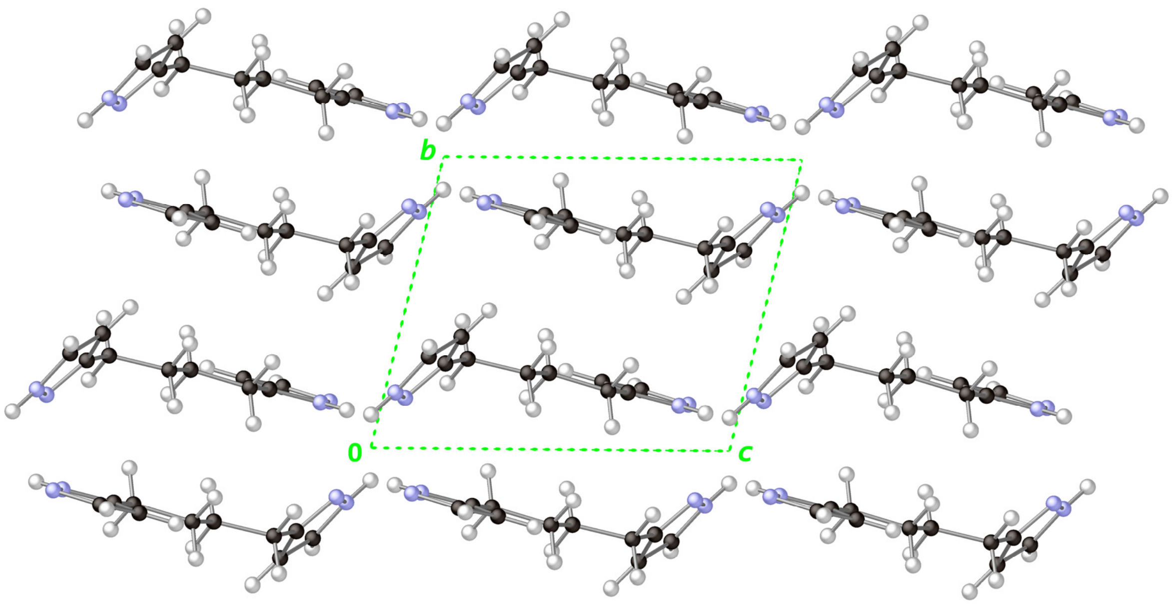

Figure S17. Packing diagram of H_2**L4**.

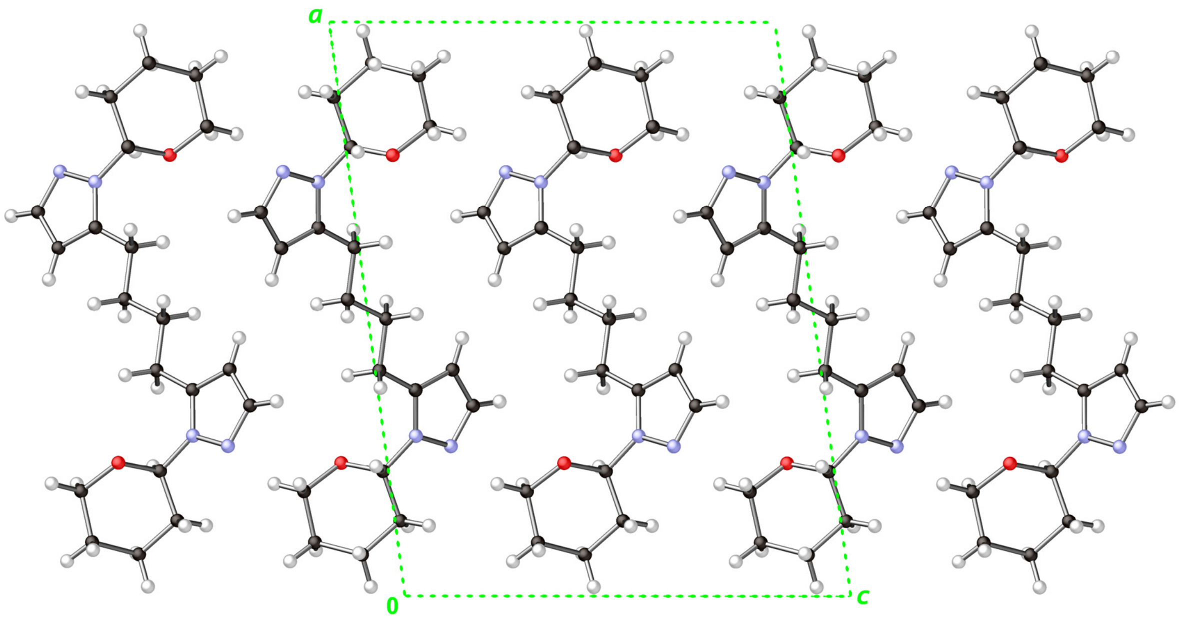

Figure S18. Packing diagram of $(THP)_2$**L4** (only one position is shown for the disordered THP-moieties).

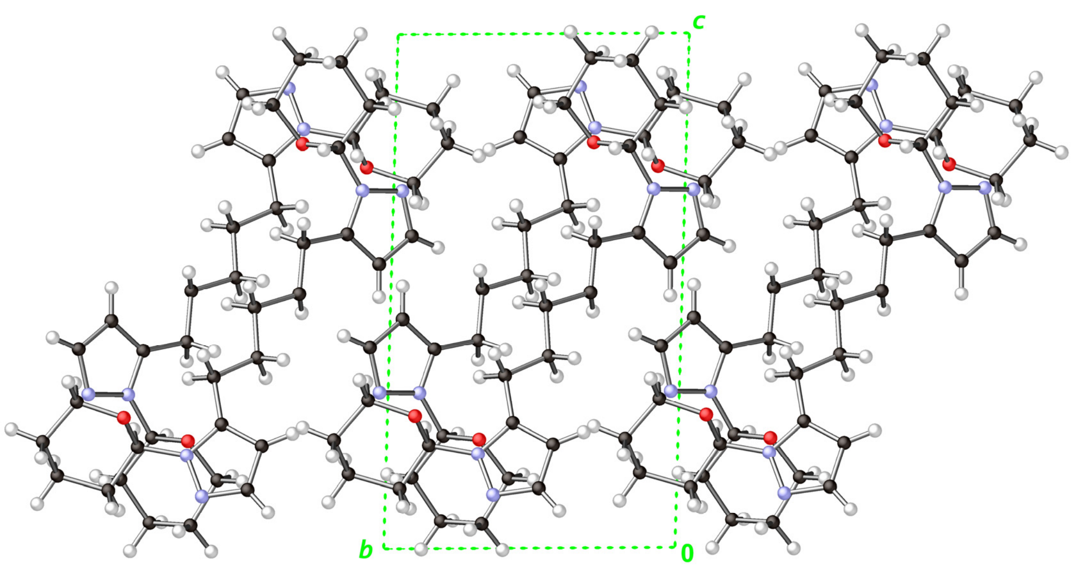

Figure S19. Packing diagram of $(THP)_2$**L5**.

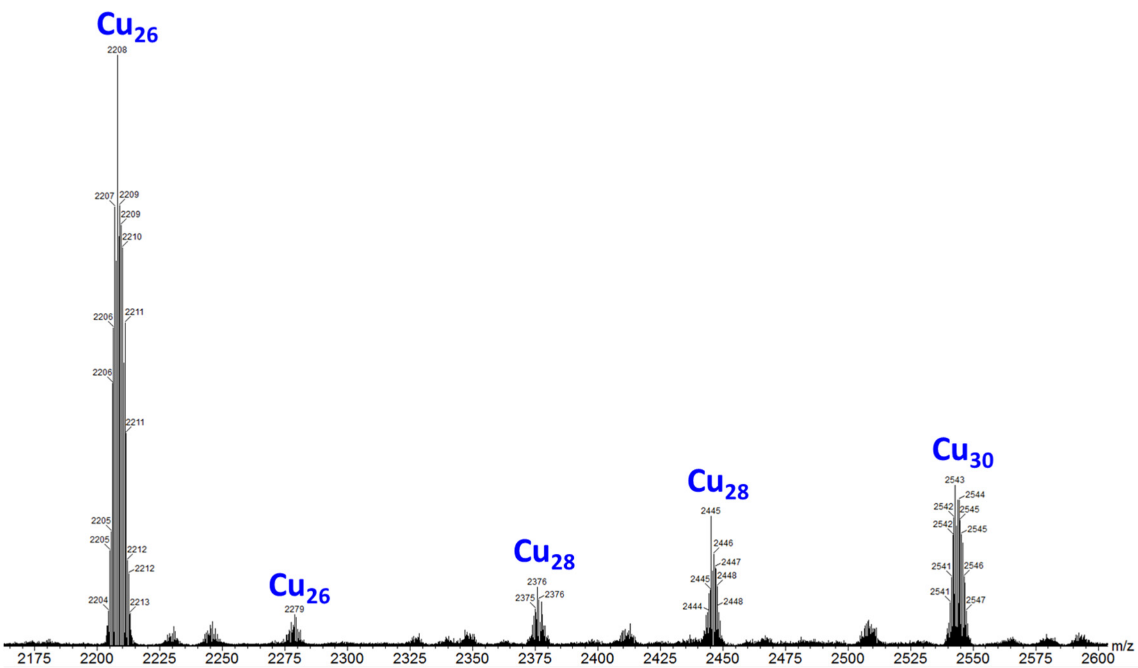

Figure S20. ESI-MS(–) spectrum in CH_3CN of the nanojar mixture formed by $Cu(NO_3)_2$, H_2**L3**, NaOH and $(Bu_4N)_2CO_3$ in a 28:14:54:2 molar ratio in THF.

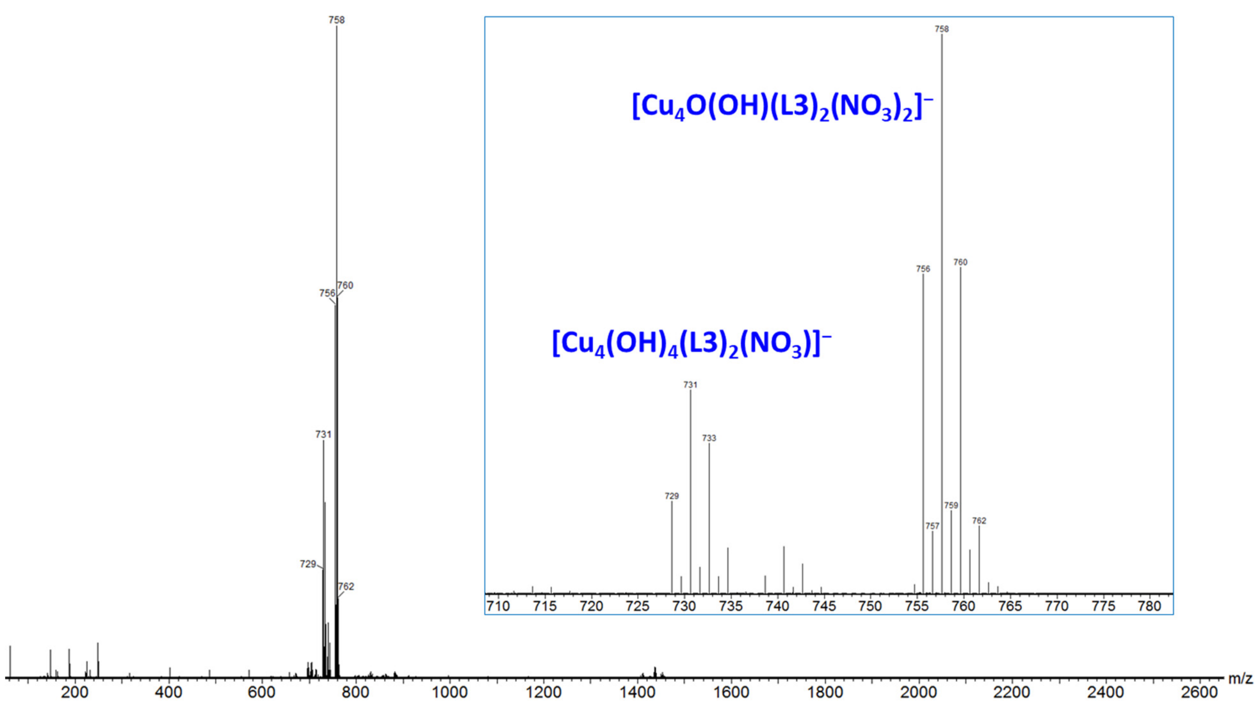

Figure S21. ESI-MS(–) spectrum in CH_3CN of the tetranuclear complex obtained from $Cu(NO_3)_2$, H_2**L3** and NaOH in a 28:14:42 molar ratio in THF.

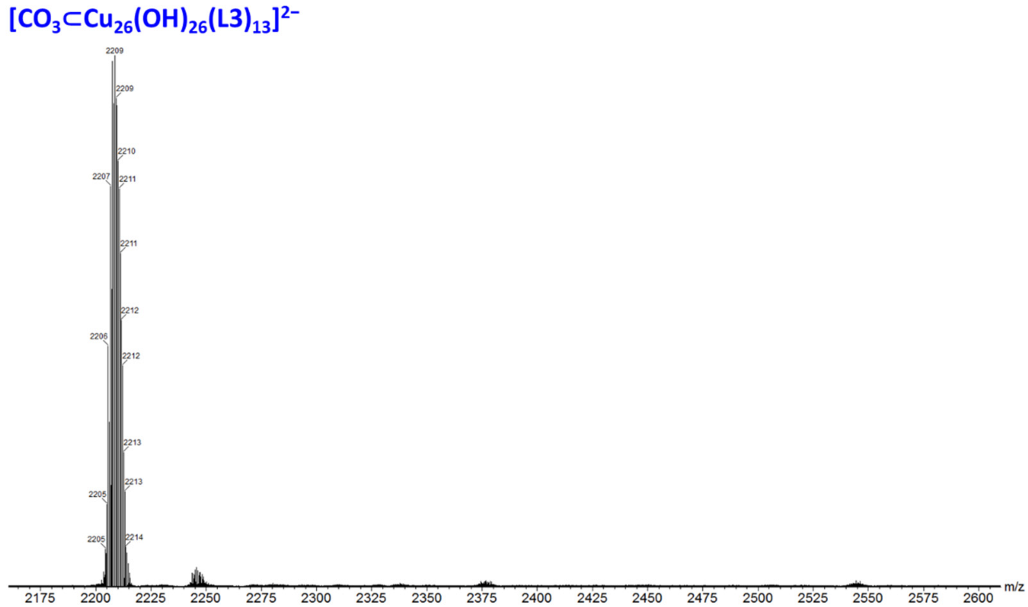

Figure S22. ESI-MS(−) spectrum in CH_3CN of the nanojar obtained from $Cu(NO_3)_2$, H_2**L3** and Bu_4NOH in a 28:28:63 molar ratio in THF.

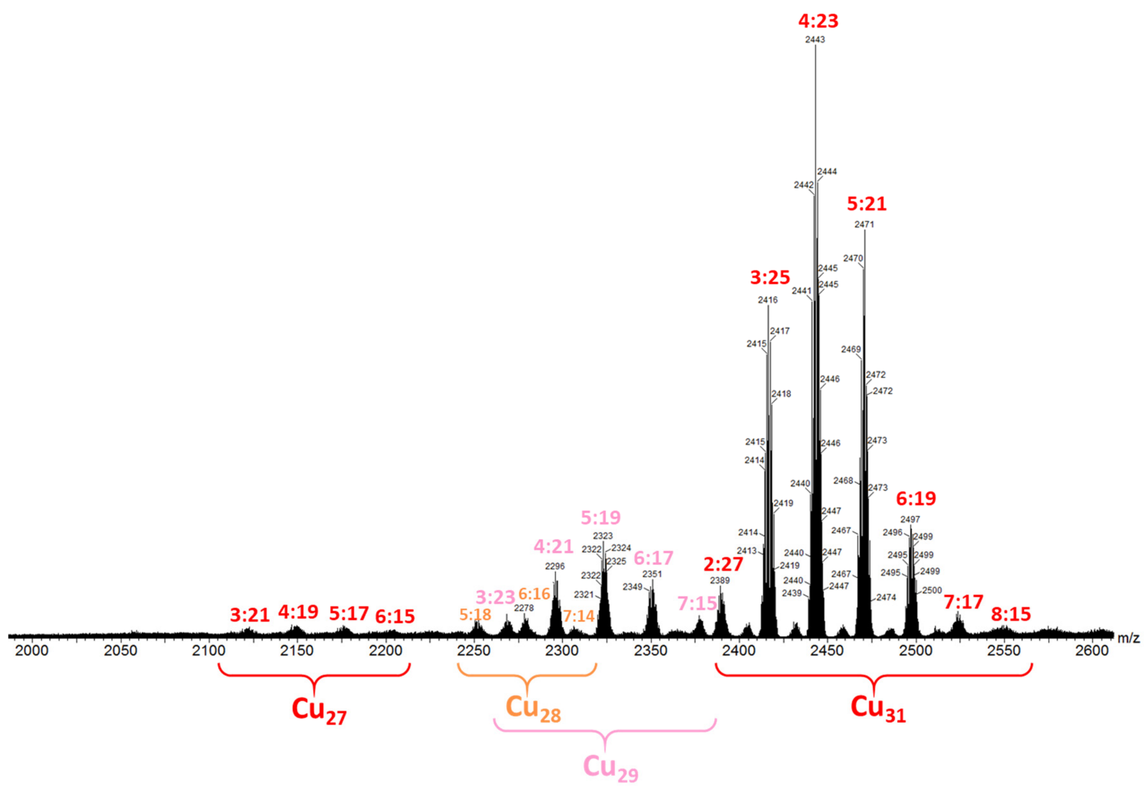

Figure S23. ESI-MS(−) spectrum in DMF of the nanojar mixture $[SO_4{\subset}Cu_n(OH)_n(\mathbf{L4})_y(pz)_{n-2y}]^{2-}$ formed by **L4** in mixture with pz (1:2 molar ratio). Cu_n abbreviations show the nuclearity of the nanojars, and the molar ratio between **L4** and pz in a given nanojar is indicated by y:n−2y.

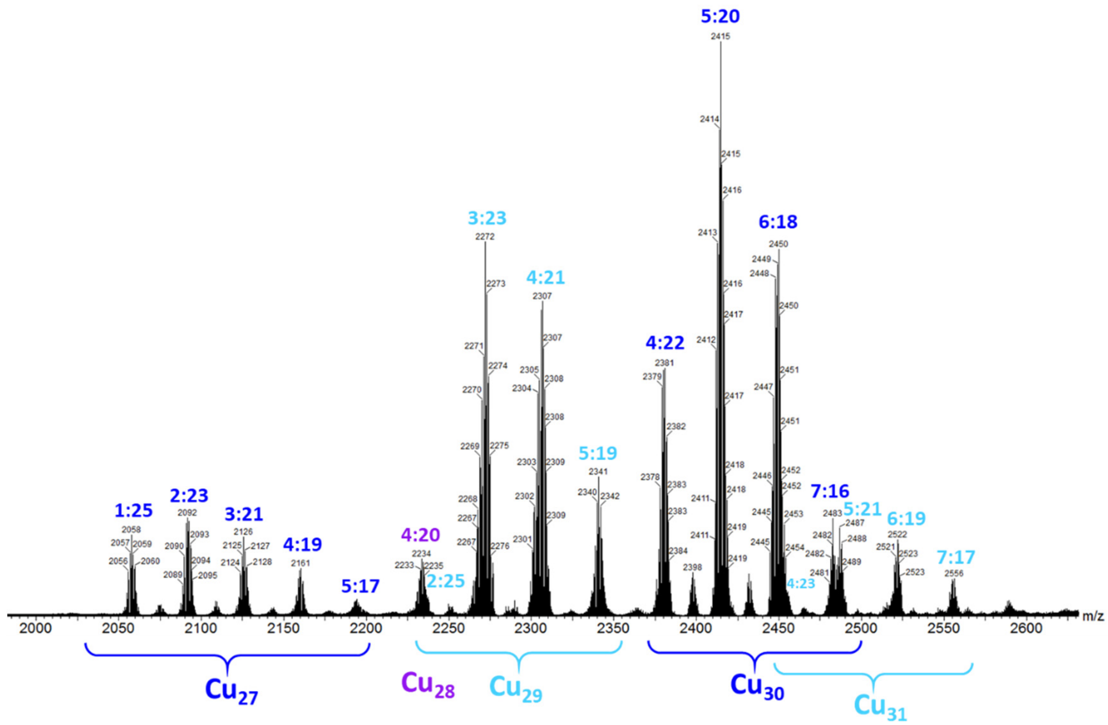

Figure S24. ESI-MS(−) spectrum in CH_3CN of the nanojar mixture $[CO_3 \subset Cu_n(OH)_n(\mathbf{L5})_y(pz)_{n-2y}]^{2-}$ formed by **L5** in mixture with pz (1:2 molar ratio). Cu_n abbreviations show the nuclearity of the nanojars, and the molar ratio between **L5** and pz in a given nanojar is indicated by y:n−2y.

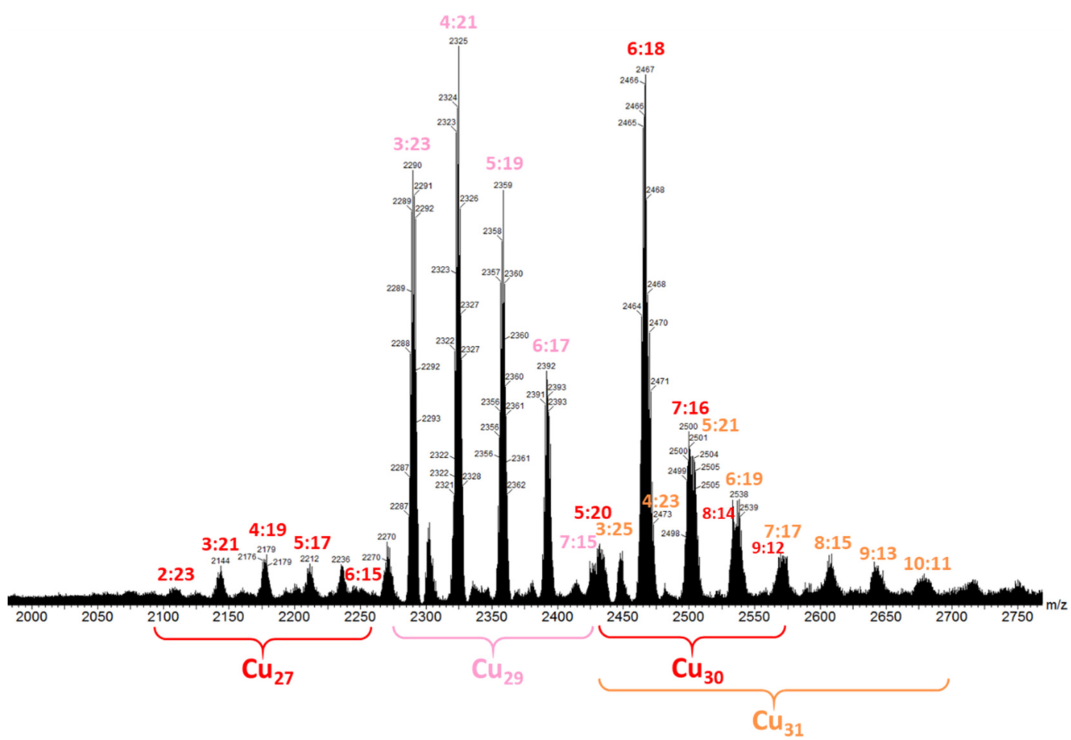

Figure S25. ESI-MS(−) spectrum in DMF of the nanojar mixture $[SO_4 \subset Cu_n(OH)_n(\mathbf{L5})_y(pz)_{n-2y}]^{2-}$ formed by **L5** in mixture with pz (1:2 molar ratio). Cu_n abbreviations show the nuclearity of the nanojars, and the molar ratio between **L5** and pz in a given nanojar is indicated by y:n−2y.

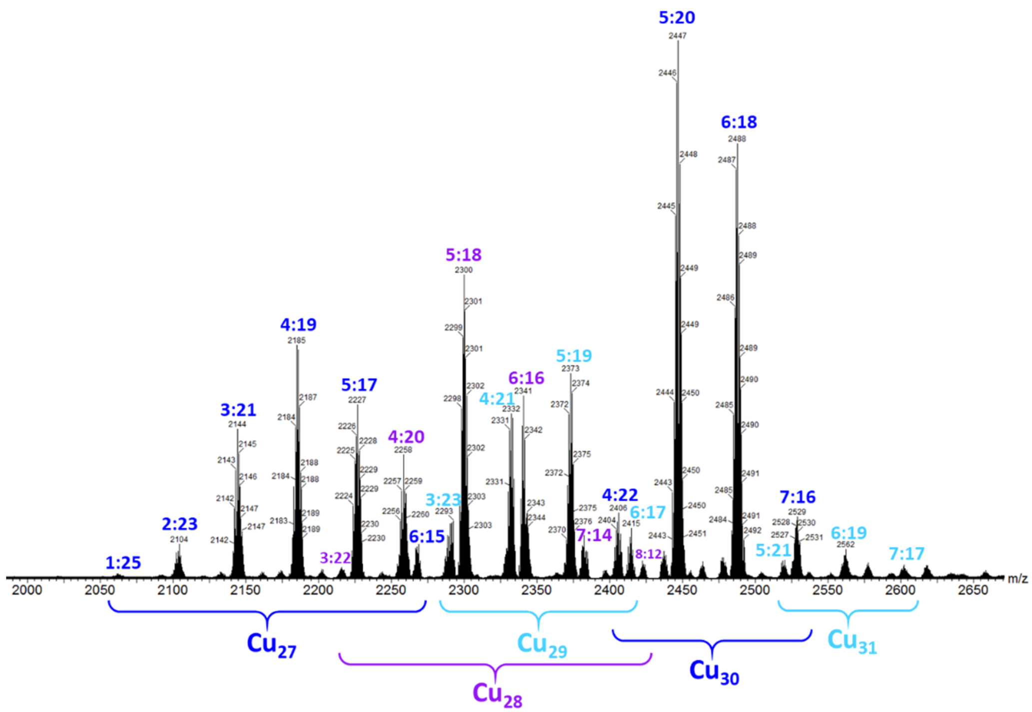

Figure S26. ESI-MS(−) spectrum in CH_3CN of the nanojar mixture $[CO_3{\subset}Cu_n(OH)_n(\mathbf{L6})_y(pz)_{n-2y}]^{2-}$ formed by **L6** in mixture with pz (1:2 molar ratio). Cu_n abbreviations show the nuclearity of the nanojars, and the molar ratio between **L6** and pz in a given nanojar is indicated by y:n−2y.

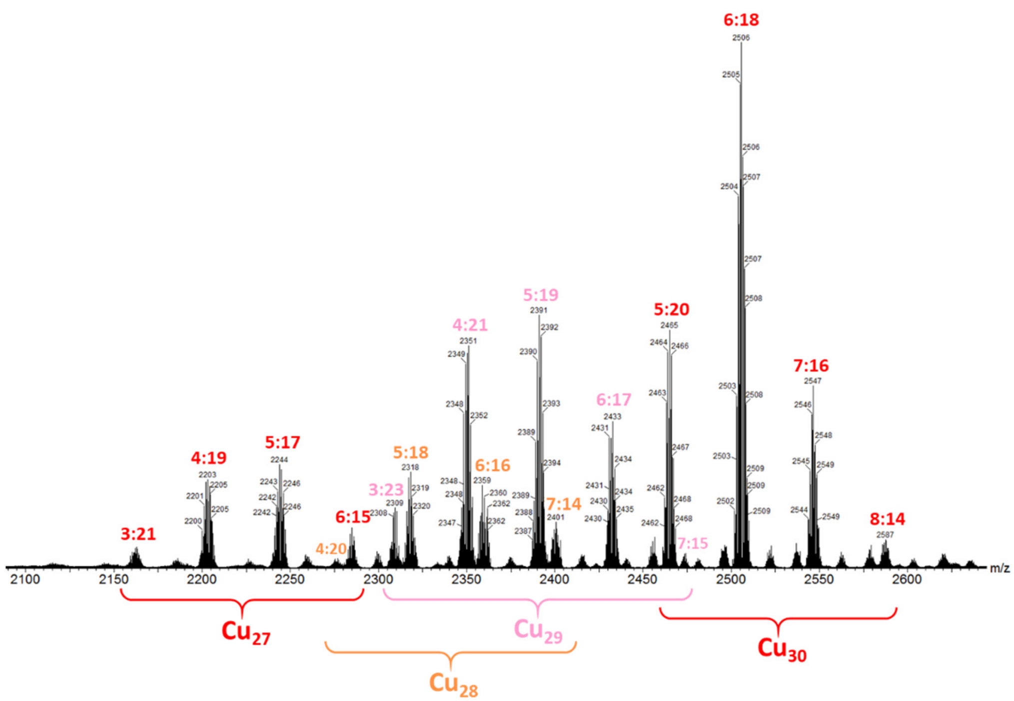

Figure S27. ESI-MS(−) spectrum in CH_3CN of the nanojar mixture $[SO_4{\subset}Cu_n(OH)_n(\mathbf{L6})_y(pz)_{n-2y}]^{2-}$ formed by **L6** in mixture with pz (1:2 molar ratio). Cu_n abbreviations show the nuclearity of the nanojars, and the molar ratio between **L6** and pz in a given nanojar is indicated by y:n−2y.

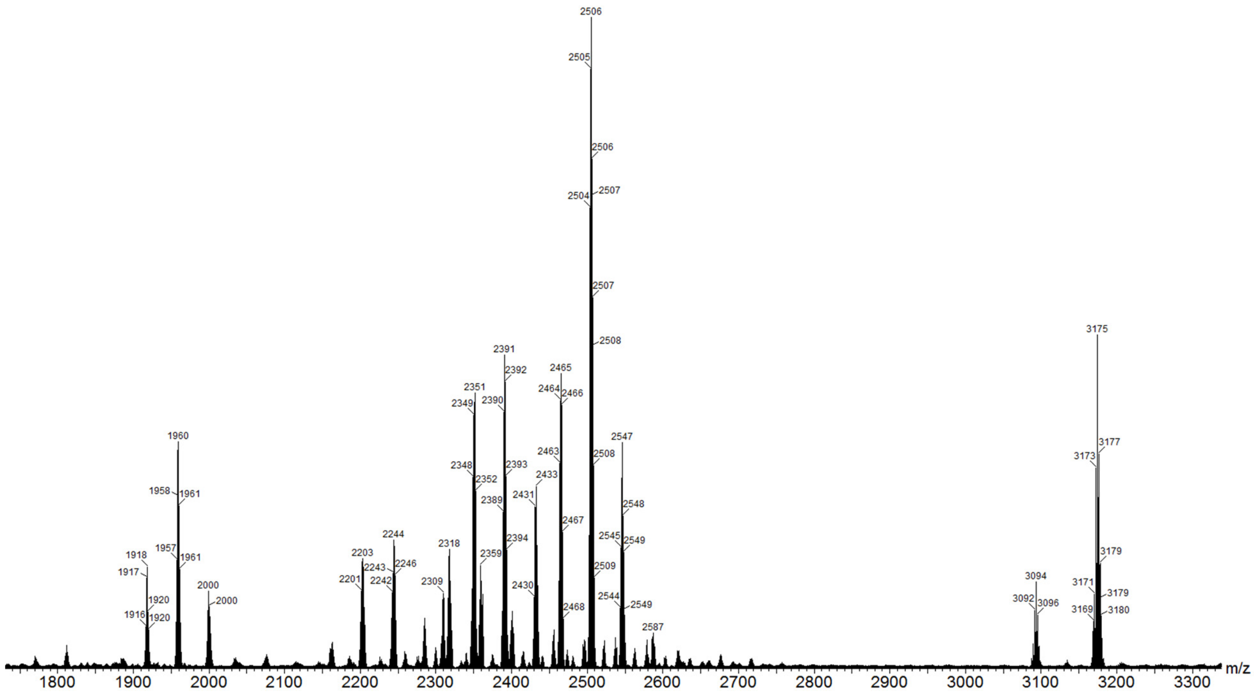

Figure S28. ESI-MS(–) spectrum in CH_3CN of the nanojar mixture $[SO_4\subset Cu_n(OH)_n(\mathbf{L6})_y(pz)_{n-2y}]^{2-}$ formed by **L6** in mixture with pz (1:2 molar ratio), showing additional peaks at *m/z* 1918–2000 and 3094–3175.

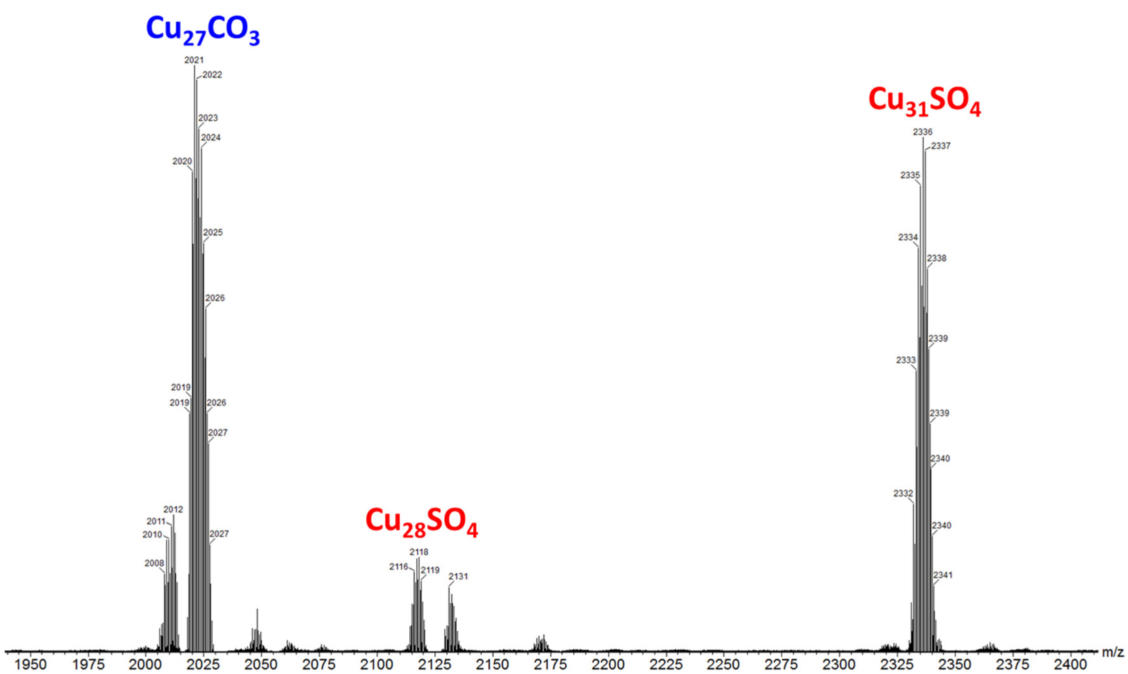

Figure S29. ESI-MS(–) spectrum in CH_3CN of the nanojar mixture obtained from $Cu(NO_3)_2$, Hpz, NaOH, Bu_4NOH and an equimolar mixture of $(Bu_4N)_2CO_3$ and $(Bu_4N)_2SO_4$ in THF.

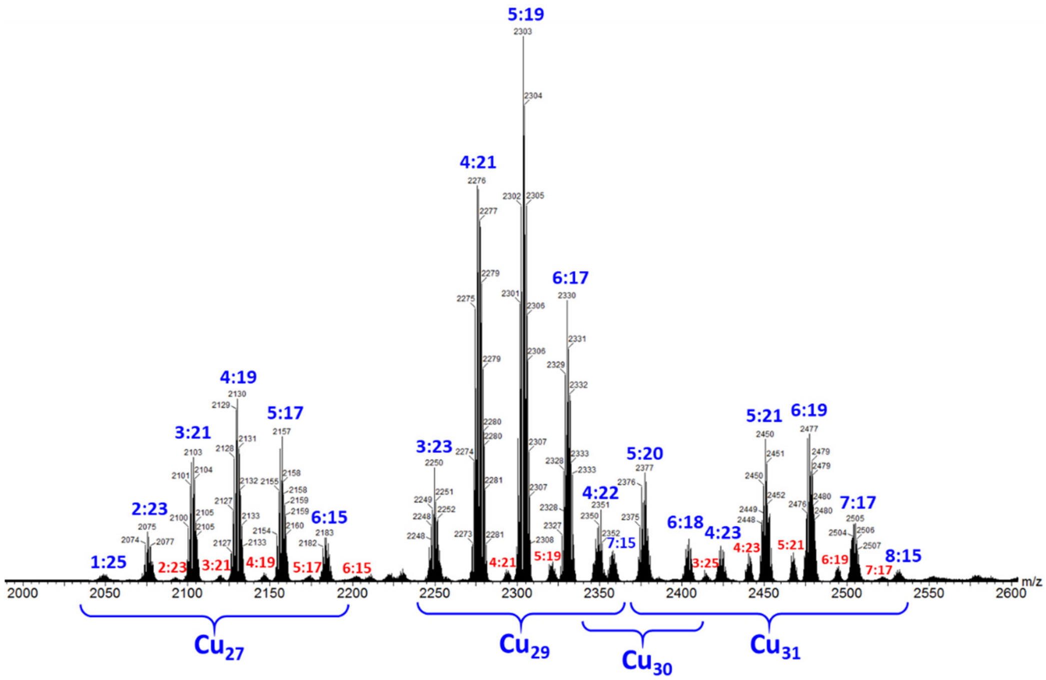

Figure S30. ESI-MS(–) spectrum in CH_3CN of the nanojar mixture $[CO_3/SO_4 \subset Cu_n(OH)_n(\mathbf{L4})_y(pz)_{n-2y}]^{2-}$ formed by **L4** in mixture with pz (1:2 molar ratio) and an equimolar mixture of $(Bu_4N)_2CO_3$ and $(Bu_4N)_2SO_4$ in THF. Cu_n abbreviations show the nuclearity of the nanojars, and the molar ratio between **L4** and pz in a given nanojar is indicated by y:n–2y.

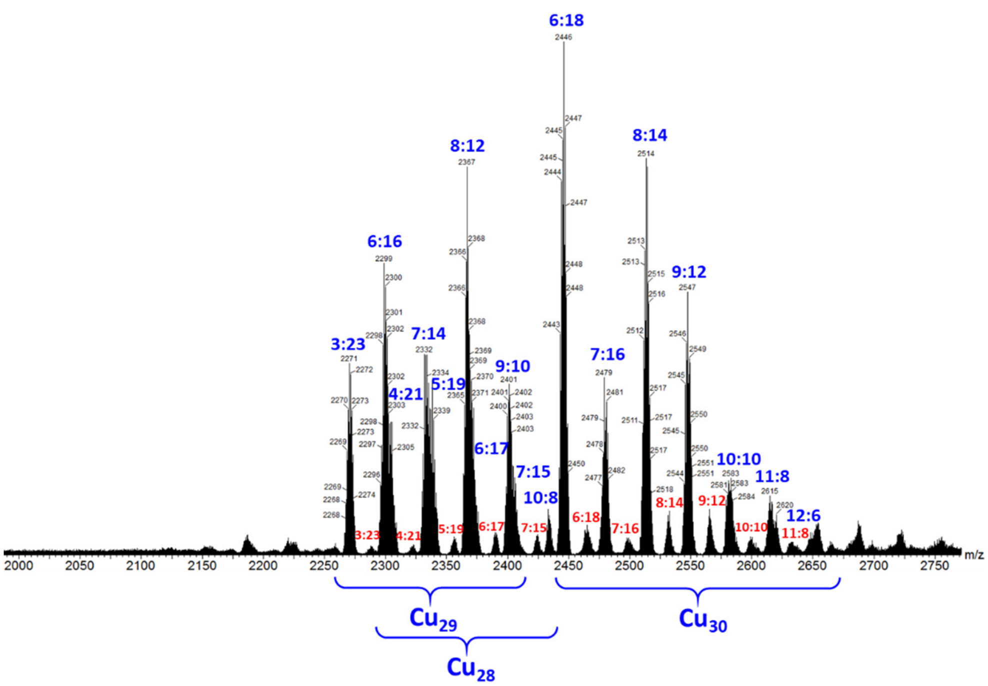

Figure S31. ESI-MS(–) spectrum in CH_3CN of the nanojar mixture $[CO_3/SO_4 \subset Cu_n(OH)_n(\mathbf{L5})_y(pz)_{n-2y}]^{2-}$ formed by **L5** in mixture with pz (1:2 molar ratio) and an equimolar mixture of $(Bu_4N)_2CO_3$ and $(Bu_4N)_2SO_4$ in THF. Cu_n abbreviations show the nuclearity of the nanojars, and the molar ratio between **L5** and pz in a given nanojar is indicated by y:n–2y.

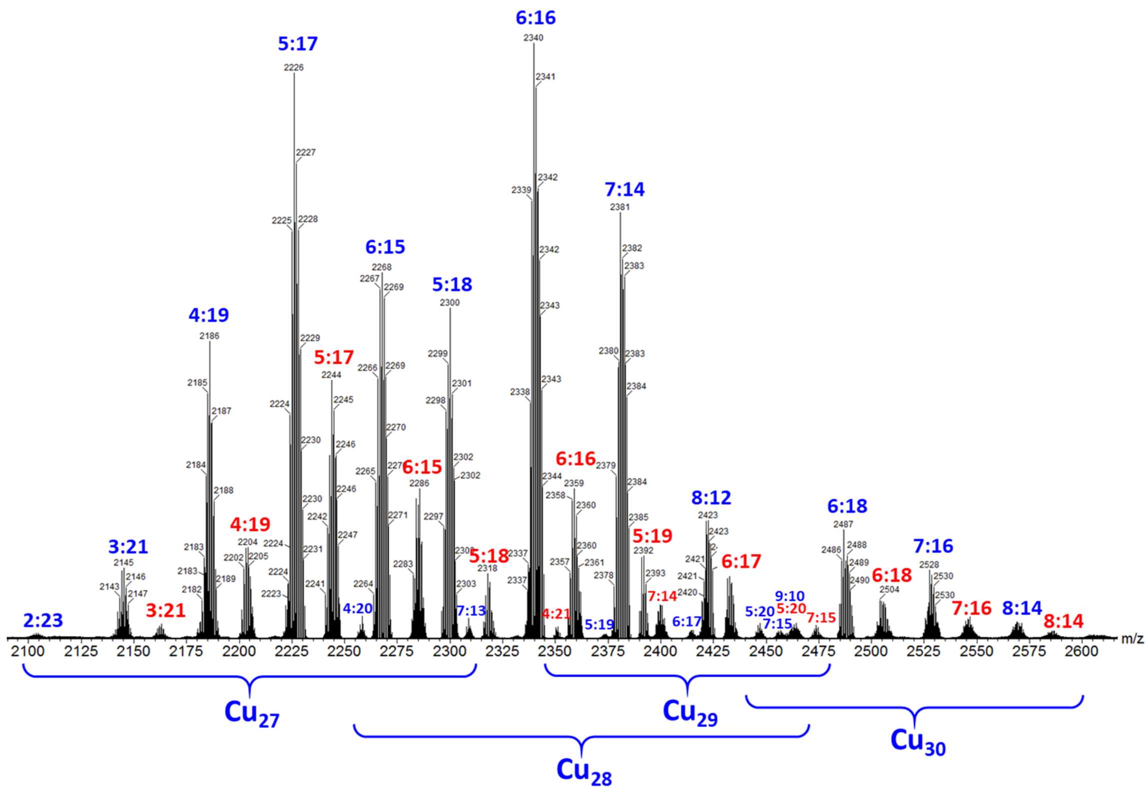

Figure S32. ESI-MS(–) spectrum in CH_3CN of the nanojar mixture $[CO_3/SO_4 \subset Cu_n(OH)_n(\mathbf{L6})_y(pz)_{n-2y}]^{2-}$ formed by **L6** in mixture with pz (1:2 molar ratio) and an equimolar mixture of $(Bu_4N)_2CO_3$ and $(Bu_4N)_2SO_4$ in THF. Cu_n abbreviations show the nuclearity of the nanojars, and the molar ratio between **L6** and pz in a given nanojar is indicated by y:n–2y.